Inorganic Chemistry

Forum Article

pubs.acs.org/IC

Structural Optimization of Zn(II)-Activated Magnetic Resonance Imaging Probes

Lauren M. Matosziuk,[†] Jonathan H. Leibowitz,[†] Marie C. Heffern,[†] Keith W. MacRenaris,[†] Mark A. Ratner,*[,‡] and Thomas J. Meade*[,†]

[†]Departments of Chemistry, Molecular Biosciences, Neurobiology, Biomedical Engineering, and Radiology, and [‡]Department of Chemistry, and Materials Science and Engineering, Northwestern University, Evanston, Illinois 60208-3113, United States

Supporting Information

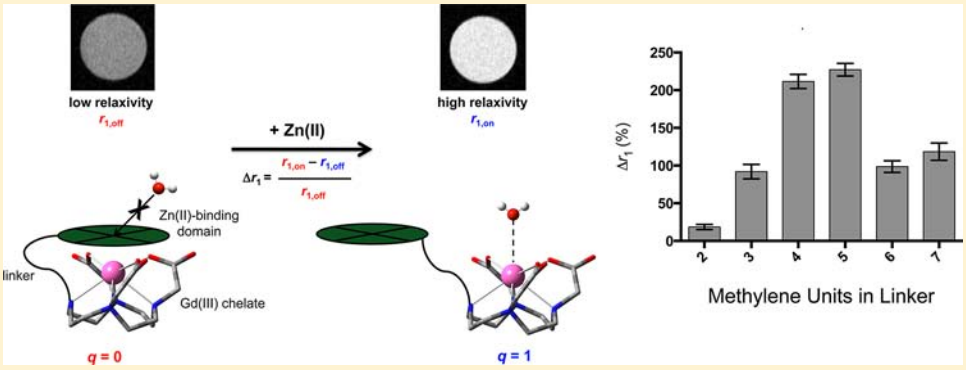

ABSTRACT: We report the structural optimization and mechanistic investigation of a series of bioactivated magnetic resonance imaging contrast agents that transform from low relaxivity to high relaxivity in the presence of Zn(II). The change in relaxivity results from a structural transformation of the complex that alters the coordination environment about the Gd(III) center. Here, we have performed a series of systematic modifications to determine the structure that provides the optimal change in relaxivity in response to the presence of Zn(II). Relaxivity measurements in the presence and absence of Zn(II) were used in conjunction with measurements regarding water access (namely, number of water molecules bound) to the Gd(III) center and temperature-dependent ^{13}C NMR spectroscopy to determine how the coordination environment about the Gd(III) center is affected by the distance between the Zn(II)-binding domain and the Gd(III) chelate, the number of functional groups on the Zn(II)-binding domain, and the presence of Zn(II). The results of this study provide valuable insight into the design principles for future bioactivated magnetic resonance probes.

INTRODUCTION

Molecular imaging is revolutionizing basic science and diagnostic medicine, providing scientists and physicians the ability to noninvasively detect and characterize an array of anatomical and biological features in animals and patients.[1−7] The primary goal of molecular imaging is to monitor and quantify specific physiological events in vivo, which is accomplished using a variety of imaging modalities such as fluorescence microscopy/endoscopy,[8−11] positron emission tomography,[12−14] single-photon emission computed tomography,[13] ultrasound,[15,16] and magnetic resonance imaging (MRI).[1,2,17] Among these imaging modalities, MRI is particularly attractive because it provides high spatial and temporal resolution, excellent soft tissue contrast, and unlimited penetration depth without using ionizing radiation or radioactive probes.

Although MRI can inherently provide physiological information about blood flow (MRA), blood oxygenation (BOLD), and brain activity (fMRI), MRI contrast agents are necessary for true molecular imaging. Specifically, Gd(III)-based contrast agents are employed in more than 10 million clinical MRI scans each year.[18] These agents shorten the longitudinal relaxation time (T_1) of water protons, providing increased image contrast in target tissues that are magnetically similar but histologically distinct. To utilize these contrast agents in vivo, Gd(III) must be chelated to prevent the release of the free ion. The efficiency of these agents [or relaxivity (r_1)] is dependent primarily on this chelate structure, which not only binds Gd(III), thus attenuating the latent toxicity of the free ion, but allows for further chemical modification. This permits researchers an opportunity to develop MRI contrast agents for molecular imaging that are conditionally activated by a selected biological event.[19−22] In these cases, the agent is transformed from low relaxivity (dark in the acquired image) to high relaxivity (brighter in the acquired image).

Special Issue: Metals in Medicine and Health

Received: March 19, 2013
Published: June 18, 2013

   dx.doi.org/10.1021/ic400681j | *Inorg. Chem.* 2013, 52, 12250−12261

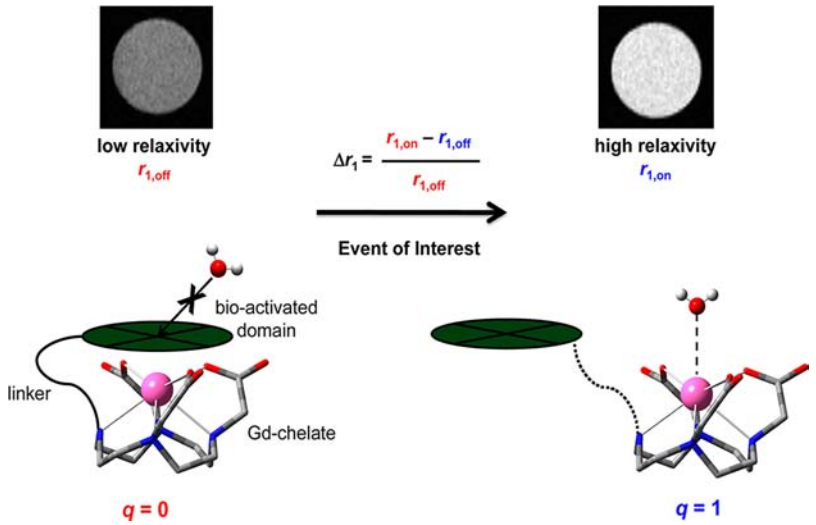

Figure 1. *q*-modulated contrast agent conditionally activated, transforming from a low-relaxivity, $q = 0$ state (left) to a higher-relaxivity, $q = 1$ state (right) in response to a biological EOI. The efficacy of the agent is largely determined by the percent change in relaxivity (Δr_1); the greater the value of Δr_1, the greater the degree of observed contrast after the EOI has occurred. The change in relaxivity can be optimized by reducing the relaxivity of the agent prior to the EOI ($r_{1,off}$) or by increasing the relaxivity after the EOI has occurred ($r_{1,on}$).

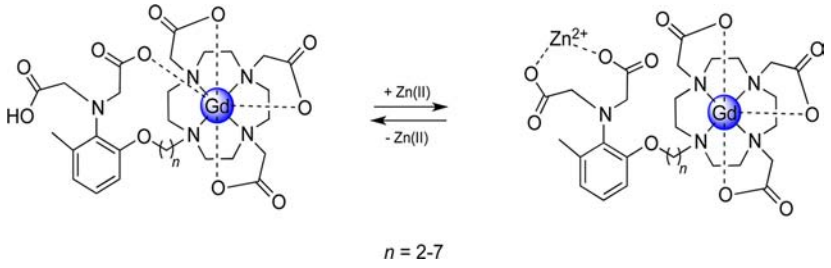

Figure 2. Model system used in this study as the Zn(II)-activated contrast agent Gd-***n***, where *n* is the number of C atoms in the aliphatic chain connecting the Zn(II)-binding domain to the Gd(III) chelate. In the absence of Zn(II), the acetate groups of the Zn(II)-binding domain coordinate to the Gd(III) center, restricting water access to create a low-relaxivity, $q = 0$ state. In the presence of Zn(II), the acetate groups preferentially coordinate to Zn(II), leaving an open site on Gd(III) for water coordination, resulting in a high-relaxivity, $q = 1$ state. The larger the change in relaxivity upon the addition of Zn(II), the more effective the agent.

The relaxivity of a T_1 contrast agent is largely determined by the number of water molecules bound to Gd(III) (q), the rate of exchange between the bound water and the bulk solvent ($1/\tau_m$), and the rate at which the molecule tumbles in solution ($1/\tau_r$).[23] We pioneered the development of *q*-modulated MRI probes, and since that time, a number of groups have developed contrast agents that respond to a wide variety of biological stimuli including enzyme activity,[19,21,24−29] ion concentration,[20,22,30−35] and pH[36−40] (Figure 1). These *q*-modulated agents consist of three primary domains: (i) a Gd(III)-containing complex to reduce T_1 and therefore generate MRI contrast, (ii) a bioactivated domain, and (iii) a chemical linkage between the two. The Gd(III)-containing moiety generally consists of a chelate that is kinetically inert.[41] The structure of the bioactivated domain is determined by the biological event of interest (EOI) the agent is designed to detect (e.g., an enzyme substrate or ion-binding domain). The design of the linker is paramount because the linker determines how the chelate and bioactivated domain interact, ultimately determining the efficacy and sensitivity of the probe. This interaction must be such that water access to the paramagnetic ion is restricted in the absence of the EOI, creating a low-relaxivity, $q = 0$ state. In response to the EOI, the probe is designed to undergo a structural transformation to allow water access to Gd(III), creating a high-relaxivity, $q = 1$ state. The greater the difference in the relaxivity of the probe before and after the EOI (Δr_1), the more sensitive the probe is for molecular imaging applications.

Because of the complex interaction between the Gd(III) chelate and the bioactivated domain, *q*-modulated agents are sensitive to minute alterations in chemical structure, particularly changes in the length and flexibility of the linker.[17,20,22,26] For example, an enzymatically activated MRI probe known as EGad showed a 20% increase in relaxivity in the presence of β-galactosidase.[21] In subsequent generations of this class of probes, the increase in r_1 was more than doubled by the addition of a single methyl group to the linkage between the chelate and the enzyme substrate.[42,43] Predicting the chemical linkage between the chelate and the bioactivated domain that will produce the optimal change in relaxivity is a significant challenge. Moreover, the multistep synthesis of the complex ligands for these conditionally activated agents makes empirical structural optimization prohibitively time-consuming.[19−21,26]

Therefore, the primary goal of this work is to develop a thorough understanding of how bioactivated domains can restrict water access prior to the EOI and determine how this interaction is modulated by systematic structural variation of the linkers employed. We have chosen a model system that is a class of Zn(II)-activated agents termed Gd-***n***,[22] where *n* is the number of C atoms in the aliphatic linker between the chelate

dx.doi.org/10.1021/ic400681j | *Inorg. Chem.* 2013, 52, 12250−12261

Scheme 1. Synthesis of Gd-*n*[a]

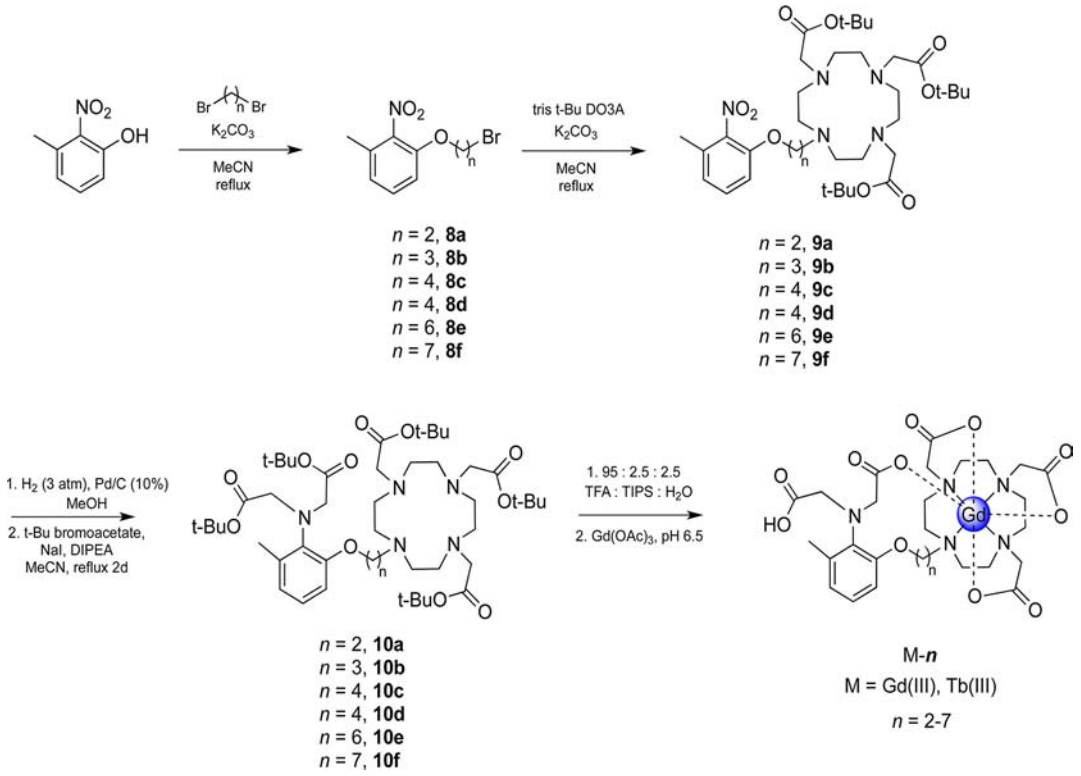

[a]The Tb(III) analogues of each compound were synthesized in a similar manner but were metalated with $Tb(OAc)_3$ in the final step. The synthesis of the ^{13}C-labeled Eu(III) analogues diverged from this scheme following hydrogenation of the nitro group; 2-^{13}C-labeled ethyl bromoacetate was added in place of unlabeled *tert*-butyl bromoacetate, precipitating the need for an additional deprotection step. Following cleavage of the *t*-Bu esters with TFA, the ethyl esters were removed using 1 M NaOH. The fully deprotected ligand was then metalated with $EuCl_3$.

and the Zn(II)-binding domain (Figure 2). In the absence of Zn(II), the acetate groups of the Zn(II)-binding domain coordinate to the Gd(III) ion, restricting water access. In the presence of Zn(II), these acetate groups preferentially bind to Zn(II), opening a coordination site on the Gd(III) ion for water access and increasing q and, in turn, r_1.

This series of q-modulated agents was chosen for several reasons. First, compared to other q-modulated agents, systematic synthetic modification to Gd-***n*** is relatively straightforward. The linkage between the chelate and the bioactivated domain can be altered by changing the length of the dibromoalkane used in the first step of the synthesis (Scheme 1). Second, minor structural modifications to the system have a significant effect on the complex's relaxivity in both the presence and absence of Zn(II). Previous work has shown that extending the linker between the chelate and the Zn(II)-binding domain from two to three methylene units had a dramatic effect on Δr_1.[22] Third, this class of agents was chosen for its biological relevance. In the process of investigating the series of complexes, we have structurally optimized the probes for maximal Δr_1, enhancing its potential as an in vivo probe for the detection of Zn(II). Significant changes in Zn(II) concentration have been associated with a number of biological processes such as insulin production in β-islet cells,[35,44] Alzheimer's disease,[45−47] epileptic seizure,[48] stroke,[47,49−51] and prostate cancer.[52,53]

The synthesis and characterization of the Zn(II)-activated MRI contrast agents Gd-**2** and Gd-**3** have been reported previously.[22] Here, we have extended this series of agents, making systematic structural modifications to examine how such changes affect the agent's response to Zn(II) (Figure 1). The relaxivity of each agent was measured in both the presence and absence of Zn(II) to determine the relationship between the linker length and Δr_1. Further characterization methods were used to determine Δq and its relationship to the variation in Δr_1 as a function of the linker length. Temperature-dependent NMR was used to examine ^{13}C-labeled complexes of three of these agents (n = 2, 4, and 6) to investigate the interaction between the acetate groups of the Zn(II)-binding domain and the Gd(III) ion (Figure 6).

MATERIALS AND METHODS

Synthesis and Purification. $Gd(OAc)_3$, $EuCl_3$, 10% Pd/C, and cyclen were purchased from Strem Chemicals. $Tb(OAc)_3$ and K_2CO_3 were purchased from Alfa Aesar. NaI was purchased from Mallinckrodt. 2-^{13}C-Ethyl bromoacetate was purchased from Cambridge Isotope Laboratories. All other chemicals were obtained from Sigma Aldrich and used without further purification. Thin-layer chromatography (TLC) was performed on EMD 60F 254 silica gel plates and visualized using UV light and iodoplatinate stain. Standard-grade, 60 Å, 230−400 mesh silica gel (Sorbent Technologies) was used for flash column chromatography. Unless otherwise noted, ^1H and ^{13}C NMR were acquired on a Bruker Avance III 500 MHz NMR spectrometer. A Varian 1200 L single-quadrupole mass spectrometer was used to acquire electrospray ionization mass spectrometry (ESI-MS) spectra. Semipreparative high-performance liquid chromatography (HPLC) was performed on a Waters 19 × 150 mm 5 μm XBridge Prep C18 column. Analytical HPLC mass spectrometer was performed using a Waters 4.6 × 150 mm 5 μm XBridge C18 column using the Varian Prostar 500 system equipped with a Varian 380 LC ELSD system, a Varian 363 fluorescence detector, and a Varian 335 UV−vis detector.

dx.doi.org/10.1021/ic400681j | *Inorg. Chem.* 2013, 52, 12250−12261

Similar procedures were used for the synthesis of **8a**−**8f**, **9a**−**9f**, and **10a**−**10f**. Representative procedures for each step of the synthesis of Gd-**2** are described below.

*1-(2-Bromoethoxy)-3-methyl-2-nitrobenzene (**8a**).* 3-Methyl-2-nitrophenol (1 g, 6.53 mmol) was dissolved in acetonitrile (75 mL), producing a clear, bright yellow solution. K_2CO_3 (3.6 g, 32.65 mmol) was added, and the reaction stirred until the color darkened to a deep red. Dibromoethane (6.10 g, 32.65 mmol) was added and the reaction refluxed overnight. Completion of the reaction was confirmed via TLC (15% ethyl acetate/hexanes), at which point the reaction mixture became pale yellow. The reaction mixture was filtered and the solvent evaporated from the filtrate to yield a yellow oil. The crude product was purified on a silica gel column, eluting with 5% ethyl acetate/hexanes, producing a pale-yellow oil (1.25 g, 74%). ^{1}H NMR (500 MHz, $CDCl_3$): δ 7.29 (t, J = 8.1 Hz, 1H), 6.87 (dd, J = 14.1 and 8.1 Hz, 2H), 4.33 (t, J = 6.4 Hz, 2H), 3.57 (t, J = 6.4 Hz, 2H), 2.28 (s, 3H). ^{13}C NMR (126 MHz, $CDCl_3$): δ 149.27, 142.37, 131.28, 130.76, 123.56, 111.47, 69.20, 28.10, 17.00.

*1-(3-Bromopropoxy)-3-methyl-2-nitrobenzene (**8b**).* Previously reported in ref 30.

*1-(4-Bromobutoxy)-3-methyl-2-nitrobenzene (**8c**).* Yield: 85%. ^{1}H NMR (500 MHz, $CDCl_3$): δ 7.45−7.13 (m, 1H), 6.95−6.67 (m, 2H), 4.08 (t, J = 5.8 Hz, 2H), 3.46 (t, J = 6.4 Hz, 2H), 2.30 (s, 3H), 2.08−1.88 (m, 4H). ^{13}C NMR (126 MHz, $CDCl_3$): δ 150.01, 142.21, 131.02, 130.66, 122.68, 110.86, 68.23, 33.46, 29.00, 27.48, 16.98.

*1-[(5-Bromopentyl)oxy]-3-methyl-2-nitrobenzene (**8d**).* Yield: 87%. ^{1}H NMR (500 MHz, $CDCl_3$): δ 7.20 (t, J = 8.1 Hz, 1H), 6.77 (dd, J = 8.1 and 3.8 Hz, 2H), 3.97 (t, J = 6.2 Hz, 2H), 3.35 (t, J = 6.8 Hz, 2H), 2.22 (s, 3H), 1.88−1.77 (m, 2H), 1.77−1.67 (m, 2H), 1.57−1.42 (m, 2H). ^{13}C NMR (126 MHz, $CDCl_3$): δ 150.13, 142.24, 130.94, 130.62, 122.53, 110.87, 68.99, 33.59, 32.29, 28.06, 24.59, 16.97.

*1-[(6-Bromohexyl)oxy]-3-methyl-2-nitrobenzene (**8e**).* Yield: 84%. ^{1}H NMR (500 MHz, $CDCl_3$): δ 7.39−7.02 (m, 1H), 6.84 (t, J = 7.6 Hz, 2H), 4.04 (t, J = 6.2 Hz, 2H), 3.42 (t, J = 6.8 Hz, 2H), 2.29 (s, 3H), 1.99−1.82 (m, 2H), 1.82−1.72 (m, 2H), 1.47 (m, 4H). ^{13}C NMR (126 MHz, $CDCl_3$): δ 150.21, 142.26, 130.91, 130.60, 122.44, 110.89, 69.10, 33.89, 32.61, 28.71, 27.76, 25.06, 16.97.

*1-[(7-Bromoheptyl)oxy]-3-methyl-2-nitrobenzene (**8f**).* Yield: 92%. ^{1}H NMR (500 MHz, $CDCl_3$) δ 7.27 (t, J = 8.0 Hz, 1H), 6.83 (t, J = 8.6 Hz, 2H), 4.03 (t, J = 6.3 Hz, 2H), 3.41 (t, J = 6.8 Hz, 2H), 2.29 (s, 3H), 1.86 (dd, J = 8.0 and 6.6 Hz, 2H), 1.76 (dd, J = 8.2 and 6.2 Hz, 2H), 1.50−1.31 (m, 6H). ^{13}C NMR (126 MHz, $CDCl_3$): δ 150.24, 142.26, 130.87, 130.58, 122.38, 110.89, 69.24, 34.05, 32.66, 28.75, 28.36, 28.02, 25.69, 16.96.

*1-Methyl-2-nitro-3-(ethoxybenzyl)tri-tert-butyl-DO3A (**9a**).* t-Bu_3-DO3A (3.82 g, 6.42 mmol) was prepared according to a literature procedure[54] and dissolved in acetonitrile (75 mL). Following the addition of K_2CO_3 (3.54 g, 25.66 mmol) and **8a** (2.51 g, 9.62 mmol), the reaction was brought to 75 °C and allowed to reflux overnight. Upon completion (confirmed via MS), the reaction mixture was filtered and the solvent evaporated. The resulting dark-yellow oil was purified on a silica gel column, eluting with 3% methanol/dichloromethane, to yield a yellow oil (5.15 g, 77% yield). ^{1}H NMR (500 MHz, $CDCl_3$): δ 7.28−7.22 (m, 1H), 6.89 (d, J = 8.4 Hz, 1H), 6.81 (d, J = 7.7 Hz, 1H), 4.20 (t, J = 4.9 Hz, 2H), 3.41−2.20 (m, 27H), 1.35 (d, J = 8.9 Hz, 27H). ^{13}C NMR (126 MHz, $CDCl_3$): δ 172.73, 171.64, 148.78, 141.14, 130.05, 122.24, 110.42, 81.73, 81.51, 67.20, 55.62, 54.78, 52.52, 51.30, 26.87, 26.81, 15.97. ESI-MS (positive mode): m/z 694.3 (M + H$^+$), 716.3 (M + Na$^+$).

*1-Methyl-2-nitro-3-(propoxybenzyl)tri-tert-butyl-DO3A (**9b**).* Previously reported in ref 30.

*1-Methyl-2-nitro-3-(butoxybenzyl)tri-tert-butyl-DO3A (**9c**).* Yield: 51%. ^{1}H NMR (500 MHz, $CDCl_3$): δ 7.28 (t, J = 8.0 Hz, 1H), 6.84 (s, 1H), 6.82 (s, 1H), 4.05 (s, 2H), 3.64−1.81 (br m, 29H), 1.71 (q, J = 6.4 Hz, 2H), 1.43 (s, 27H). ^{13}C NMR (126 MHz, $CDCl_3$): δ 172.69, 170.08, 150.03, 142.30, 130.92, 130.86, 122.72, 111.01, 82.69, 82.47, 68.79, 56.49, 55.79, 53.91, 28.20, 27.92, 26.93, 23.16, 17.01. ESI-MS (positive mode): m/z 722.4 (M + H$^+$), 744.3 (M + Na$^+$).

*1-Methyl-2-nitro-3-[(pentyloxy)benzyl]tri-tert-butyl-DO3A (**9d**).* Yield: 63%. ^{1}H NMR (500 MHz, $CDCl_3$): δ 7.27 (t, J = 8.0 Hz, 1H), 6.85 (s, 1H), 6.83 (s, 1H), 4.01 (t, J = 6.2 Hz, 2H), 3.58−1.97 (br m, 25H), 1.89−1.66 (br m, 8H), 1.45 (m, 27H). ^{13}C NMR (126 MHz, $CDCl_3$): δ 172.82, 170.12, 150.25, 131.01, 130.78, 122.68, 111.01, 82.78, 82.41, 69.41, 55.92, 54.31, 29.02, 28.30, 28.25, 28.08, 27.96, 26.28, 24.19, 17.07. ESI-MS (positive mode): m/z 736.5 (M + H$^+$), 758.4 (M + Na$^+$).

*1-Methyl-2-nitro-3-[(hexyloxy)benzyl]tri-tert-butyl-DO3A (**9e**).* Yield: 76%. ^{1}H NMR (500 MHz, $CDCl_3$): δ 7.27 (m, 1H), 6.83 (m, 2H), 4.00 (m, 2H), 3.46−1.93 (br m, 29H), 1.79−1.69 (m, 4H), 1.47−1.4 (m, 27H), 1.32−1.23 (m, 2H). ^{13}C NMR (126 MHz, $CDCl_3$): δ 172.72, 170.55, 170.08, 150.25, 142.29, 130.92, 130.76, 122.55, 110.95, 82.46, 81.93, 69.16, 55.85, 54.44, 28.94, 28.26, 28.21, 28.02, 27.93, 27.30, 26.62, 25.92, 17.03. ESI-MS (positive mode): m/z 750.4 (M + H$^+$), 772.4 (M + Na$^+$).

*1-Methyl-2-nitro-3-[(heptyloxy)benzyl]tri-tert-butyl-DO3A (**9f**).* Yield: 73%. ^{1}H NMR (500 MHz, $CDCl_3$): δ 7.27 (m, 1H), 6.83 (m, 2H), 4.02 (dt, J = 14.8 and 6.1 Hz, 2H), 3.63−1.8 (br m, 29H), 1.78−1.67 (m, 4H), 1.49−1.39 (m, 27H), 1.37−1.20 (m, 4H). ESI-MS (positive mode): m/z 764.4 (M + H$^+$), 786.3 (M + Na$^+$).

*[[bis[(2-tert-butoxy-2-oxoethyl)amino]-3-methylphenoxy]ethyl]-tri-tert-butyl-DO3A (**10a**).* Methanol (20 mL) was used to dissolve **9a** (1.032 g, 1.49 mmol) and the solution transferred to a hydrogenator flask. A catalytic amount of 10 wt % Pd/C was added and the vessel shaken on a hydrogenation reactor overnight under 3 atm of H_2. Complete reduction of nitrophenol to the corresponding aniline compound was confirmed with ESI-MS. The reaction mixture was filtered through Celite, rinsing with 100 mL of methanol. The solvent was removed from the filtrate to yield a pink oil (819 mg, 83%), which was used without further purification. The oil was dissolved in 50 mL of acetonitrile. *N*,*N*-Diisopropylethylamine (479 mg, 3.7 mmol), *tert*-butyl bromoacetate (5.33 mg, 2.72 mmol), and NaI (408 mg, 2.72 mmol) were added, and the solution was refluxed under nitrogen for several days. The reaction was monitored by MS. An additional 1 equiv of *tert*-butyl bromoacetate (242 mg, 1.24 mmol) and NaI (204 mg, 1.24 mmol) were added every 24 h until only product was observed by MS. The mixture was then filtered and purified on a silica gel column, eluting with 0−2% methanol in dichloromethane. The product was obtained as a dark-yellow oil (460 mg, 42%) and analyzed as reported in ref 22.

Note: the following compounds were analyzed by ESI-MS only. NMR could not be used for analysis because of peak broadening resulting from the macrocycle.[55] The ^{13}C-labeled complexes were synthesized under the same conditions, using 2-^{13}C-ethyl bromoacetate in place of *tert*-butyl bromoacetate.

*[[Bis[(2-tert-butoxy-2-oxoethyl)amino]-3-methylphenoxy]-propyl]tri-tert-butyl-DO3A (**10b**).* Previously reported in ref 22.

*[[Bis[(2-tert-butoxy-2-oxoethyl)amino]-3-methylphenoxy]butyl]-tri-tert-butyl-DO3A (**10c**).* Yield: 73%. ESI-MS (positive mode): m/z 920.6 (M + H$^+$), 942.6 (M + Na$^+$).

*[[Bis[(2-tert-butoxy-2-oxoethyl)amino]-3-methylphenoxy]-pentyl]tri-tert-butyl-DO3A (**10d**).* Yield: 67%. ESI-MS (positive mode): m/z 934.6 (M + H$^+$), 956.6 (M + Na$^+$).

*[[Bis[(2-tert-butoxy-2-oxoethyl)amino]-3-methylphenoxy]hexyl]-tri-tert-butyl-DO3A (**10e**).* Yield: 89%. ESI-MS (positive mode): m/z 948.6 (M + H$^+$), 970.5 (M + Na$^+$).

*[[Bis[(2-tert-butoxy-2-oxoethyl)amino]-3-methylphenoxy]-heptyl]tri-tert-butyl-DO3A (**10f**).* Yield: 78%. ESI-MS (positive mode): m/z 962.6 (M + H$^+$), 984.6 (M + Na$^+$).

*[[Bis[(2-ethoxy-2-oxoethyl)amino]-3-methylphenoxy]ethyl]tri-tert-butyl-DO3A [**11a**; See Supporting Information (SI) Scheme 1].* Yield: 48%. ESI-MS (positive mode): m/z 838.5 (M + H$^+$), 860.4 (M + Na$^+$).

*[[Bis[(2-ethoxy-2-oxoethyl)amino]-3-methylphenoxy]butyl]tri-tert-butyl-DO3A (**11b**; See SI Scheme 1).* Yield: 44%. ESI-MS (positive mode): m/z 865.5 (M + H$^+$), 888.5 (M + Na$^+$).

*[[bis[(2-(ethoxy-2-oxoethyl)amino]-3-methylphenoxy]hexyl]tri-tert-butyl-DO3A (**11c**; See SI Scheme 1).* Yield: 63%. ESI-MS (positive mode): m/z 894.6 (M + H$^+$), 916.5 (M + Na$^+$).

dx.doi.org/10.1021/ic400681j | *Inorg. Chem.* 2013, 52, 12250−12261

*Metalation Procedure for M-**n** (M = Gd^{III}, Tb^{III}).* The *tert*-butyl-protected ligand, **10**, was dissolved in 10 mL of a solution of 95:2.5:2.5 trifluoroacetic acid (TFA)/triisopropylsilane/water and stirred for 5 h. Complete removal of the *tert*-butyl protecting groups was confirmed with ESI-MS. The TFA solution was evaporated under a stream of nitrogen, leaving a dark-yellow oil, which was brought up in 5 mL of water. The pH was adjusted to 6.5 using 1 M NaOH. $Gd(OAc)_3$ or $Tb(OAc)_3$ was added (1.5 equiv), the pH readjusted to 6.5 with NaOH (1 M), and the reaction stirred at room temperature for 3 days. During this time, the pH was readjusted to 6.5 with NaOH (1 M) as needed. Upon completion (confirmed with ESI-MS), the reaction mixture was transferred to a 50 mL centrifuge tube. The pH was raised to 11 with NaOH (1 M), causing precipitation of the remaining unreacted metal as $Gd(OH)_3$ or $Tb(OH)_3$. The mixture was centrifuged and the supernatant filtered and purified with reverse-phase semipreparative HPLC on a Waters 19 × 150 mm 5 μm XBridge Prep C18 column, eluting with a gradient of 5−25% acetonitrile in an aqueous solution of ammonium hydroxide (pH ∼10.4) over 20 min. The purity and identity of the product were confirmed using analytical HPLC-MS on a Waters 4.6 × 150 mm 5 μm XBridge C18 column, eluting with a gradient of 5−100% acetonitrile in an aqueous solution of ammonium hydroxide (pH ∼10.4) over 30 min. Retention times and ESI-MS data can be found in the SI. The solvent was evaporated from pure fractions and the residue dissolved and freeze-dried to yield a white powder.

*Metalation Procedure for ^{13}C-Labeled Eu-**n**.* For metalation of the ^{13}C-labeled Eu-***n*** complexes (Eu-***n****), several modifications were made to the procedure described above. Following removal of the *tert*-butyl protecting groups with a TFA/triisopropylsilane/water mixture, the compound was brought up in NaOH (1 M) and stirred for several hours. Complete removal of the ethyl protecting groups on the Zn(II)-binding domain was confirmed by ESI-MS after 4 h. The pH was adjusted to 6.5 with HCl (1 M), and $EuCl_3$ (1.5 equiv) was added. The solution was stirred at room temperature for 2 days. The pH was adjusted back to 6.5 with NaOH (1 M) as needed. The metal complexes were purified by HPLC, as described above. Retention times and MS data can be found in the SI.

Relaxivity. T_1 relaxation times were measured in a *N*-2-hydroxyethylpiperazine-*N*′-2-ethanesulfonic acid (HEPES) buffer (pH 7.4) at 37 °C on a Bruker mq60 NMR analyzer equipped with *Minispec V2.51 Rev.00/NT* software (Billerica, MA). An inversion-recovery pulse sequence (t1_ir_mb) was used with the following parameters: four scans per point, 10 data points for fitting, monoexponential curve fitting, phase cycling, 10 ms first pulse separation, and a recycle delay and final pulse separation $\geq 5T_1$. For each Gd(III) complex, T_1 values were measured at five different concentrations. The T_1 relaxation rate was plotted as a function of the Gd(III) concentration [determined by inductively coupled plasma mass spectrometry (ICP-MS)]; the relaxivity was determined from the slope of the linear fit.

ICP-MS. ICP-MS was performed on a computer-controlled (*Plasmalab* software) Thermo X series II inductively coupled plasma mass spectrometer (Thermo Fisher Scientific, Waltham, MA) equipped with a CETAC 260 autosampler (Omaha, NE). Each sample was acquired using one survey run (10 sweeps) and three main (peak jumping) runs (100 sweeps). The isotopes selected for analysis were ^{157,158}Gd, ^{115}In, and ^{165}Ho (chosen as internal standards for data interpolation and machine stability).

***q* Measurements.** Tb(III) analogues of each complex were synthesized to measure the number of water molecules directly coordinated to the lanthanide (q). The rate of luminescence decay for each complex was measured using a Hitachi F4500 fluorimeter (San Francisco, CA) with an excitation wavelength of 254 nm and an emission wavelength of 544 nm. A total of 25 scans were acquired, averaged, and fit to a monoexponential decay function to determine the luminescence lifetime of each complex as a 1 mM solution in either a HEPES buffer or a deuterated HEPES buffer (prepared by repeated lyophilization and resuspension in D_2O). The hydration number was determined using the following empirically determined equation:

$$q = 4.2\left(\frac{1}{\tau_{H_2O}} - \frac{1}{\tau_{D_2O}} - 0.06\right)$$

where τ_{H_2O} and τ_{D_2O} are the luminescence lifetimes in H_2O and D_2O, respectively.[56]

Zn(II) Dissociation Constant. The Zn(II) dissociation constant ($K_{D,Zn(II)}$) for each Gd-***n*** complex was measured using a competitive binding assay with FluoZin-1[57] (purchased from Life Technologies), a Zn(II)-activated fluorophore with a known Zn(II) dissociation constant (SI Figure 3).[22] A 0.1 mM solution of FluoZin-1 in a HEPES buffer was titrated into a 10 μM solution of $ZnCl_2$ in 25 μL increments. Following the addition of each aliquot, the solution was incubated at room temperature for 30 min to allow the reaction to come to equilibrium and the fluorescence intensity at 517 nm recorded using an excitation wavelength of 495 nm. This process was repeated until equilibrium was reached; i.e., the addition of FluoZin-1 produced no further change in fluorescence. Titration experiments were repeated with solutions of Gd-***n*** (either 100 or 200 μM) and $ZnCl_2$ (10 μM). The fluorescence reduction caused by the presence of Gd-***n*** was used to determine the equilibrium concentrations of each species in solution, which were subsequently used to calculate $K_{D,Zn(II)}$. See the SI for calculation details.

Temperature-Dependent NMR. Temperature-dependent ^{13}C NMR of labeled Eu-***n*** was measured on a Bruker Avance III 600 MHz spectrometer using a broadband observe probe. High concentrations of Eu-***n*** (∼10−20 mM in D_2O) and a large number of scans (20−50K, depending on the concentration) were required to obtain satisfactory spectra. After each change in the temperature, the instrument was allowed to equilibrate for 10 min before acquisition.

MRI and Relaxation Time Measurements at 7.05 T. All MRI was performed on an 89-mm-bore-size PharmaScan 7.05 T MRI spectrometer fitted with shielded gradient coils (Bruker BioSpin, Billerica, MA) using a RF RES 300 1H 089/023 quadrature transmit/receive mouse brain volume coil (Bruker BioSpin, Billerica, MA). All MRI images were acquired using *Paravision 5.0.1* software (Bruker BioSpin, Billerica, MA).

T_1-weighted images were acquired using a rapid-acquisition rapid-echo variable repetition time (RAREVTR) pulse sequence using the following parameters: RARE factor = 1, echo time = 11 ms, averages = 3, matrix size (MTX) = 128 × 128, field of view = 25 mm × 25 mm, six slices, slice thickness = 1.5 mm, interslice distance = 2.0 mm, repetition times = 15000, 10000, 8000, 6000, 3000, 1500, 1000, 750, 500, 300, 200, and 150 ms, and a total scan time of ∼3 h 45 min. T_1 values of selected regions of interest of five out of six slices were calculated using the T_1 saturation recovery monoexponential curve fitting formula provided by the image sequence analysis tool in *Paravision 5.0.1* software (Bruker BioSpin, Billerica, MA).

RESULTS AND DISCUSSION

A series of Zn(II)-responsive MRI contrast agents have been synthesized and characterized (Figure 2). Each agent consists of an acetate-based Zn(II)-binding domain conjugated to a Gd(III)-DO3A chelate by an aliphatic linker. Both the linker length (n = 2−7) and the number of acetate groups on the Zn(II)-binding domain (m = 1, 2) were varied to determine how such modifications affect the structure of the agent, its water coordination capabilities, and consequently its response to the presence of Zn(II).

The relaxation properties in both the presence and absence of Zn(II), ion selectivity, and Zn(II) sensitivity of each agent were measured to determine the effect of structural variation on the efficacy of the contrast agent. In addition, the q values in both the presence and absence of Zn(II) were measured and used in conjunction with both relaxometry data and temperature-dependent ^{13}C NMR spectroscopy to understand how the coordination geometry of the Gd(III) ion is influenced by

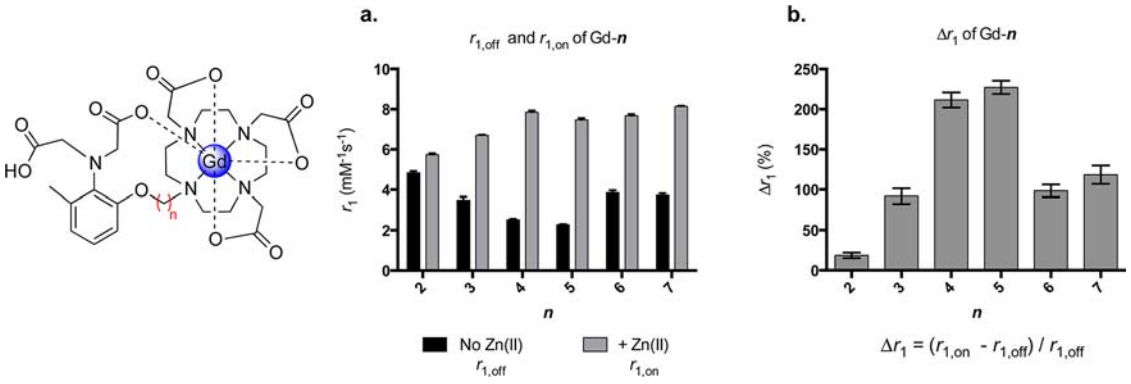

Figure 3. (a) Relaxivity (r_1) of Gd-***n*** before and after the addition of 1 equiv of Zn(II). (b) Δr_1 (%) of Gd-***n*** upon the addition of Zn(II). Relaxivity was measured in a HEPES buffer (pH 7.4) at 1.4 T, 37 °C. All measurements were performed in triplicate, and the data are presented as the average value ± standard deviation. There is a clear relationship between Δr_1 and the length of the aliphatic chain connecting the Gd(III) chelate to the Zn(II)-binding domain. This structural dependence is primarily a result of variation in r_1 prior to the addition of Zn(II) ($r_{1,off}$). For complexes in which n = 4–7, there is little variation in the relaxivity after the addition of Zn(II) ($r_{1,on}$). Complexes in which n = 4 or 5 exhibit the lowest value of $r_{1,off}$ and consequently display the largest values of Δr_1.

the linker length and how this affects the relaxation properties of the complex.

This information provides a more complete understanding of how systematic structural changes affect the metal coordination properties of this class of bioactivated contrast agents. Knowing which structural components of the system are required for creating distinct high- and low-relaxivity states will facilitate the optimization of existing bioactivated contrast agents as well as aid in the development future agents for molecular imaging.

Synthesis and Purification. Minor modifications have been made to the previously reported synthesis of Gd-***n***.[54] Methylnitrophenol was alkylated with dibromoalkane of a desired length to yield **8**. The terminal bromine was substituted with tri-*tert*-butyl-DO3A to form **9**. Nitrophenol was reduced to aniline under H_2 using a catalytic amount of 10% Pd/C. The *tert*-butyl-protected acetates of the Zn(II)-binding domain were added using 2 equiv of *tert*-butyl bromoacetate, forming **10**. Following total deprotection with TFA, the ligand was metalated with $Gd(OAc)_3$ and purified using HPLC, eluting with acetonitrile and an aqueous solution of ammonium hydroxide.

The ^{13}C-labeled analogues of Eu-**2**, Eu-**4**, Eu-**6**, and **1a**-Eu-**4** were synthesized in a similar fashion. The synthetic schemes diverge at the penultimate step, in which 2-^{13}C-ethyl bromoacetate is added in place of *tert*-butyl bromoacetate (SI Scheme 1). The *tert*-butyl esters of the DO3A moiety are then cleaved using TFA. The ethyl esters were subsequently removed using 1 M NaOH and the fully deprotected ligand metalated with $EuCl_3$.

T_1 Relaxation with and without Zn(II). The most significant physical parameter for evaluating the efficacy of bioactivated MR contrast agents is Δr_1, the change in relaxivity in response to the EOI. Larger values of Δr_1 facilitate differentiation between the "on" and "off" states of the agent, improving researchers' ability to discern whether the EOI has occurred.

r_1 of complexes Gd-**2**–Gd-**7** was measured in both the presence ($r_{1,on}$) and absence ($r_{1,off}$) of Zn(II). These values revealed a clear relationship between Δr_1 and the linker length, n (Figure 3). At 1.4 T, a maximum value of Δr_1 is achieved when n = 4 or 5, where the addition of Zn(II) causes a 200% change in r_1 from approximately 2.5 to 7.8 mM^{-1} s^{-1} (Figure 3). Complexes in which n = 3, 6, or 7 show a less substantial increase in relaxivity (near 100%); however, the addition of Zn(II) to Gd-**2** only produces a 20% increase in relaxivity.

This structural dependence of Δr_1 results primarily from variation in $r_{1,off}$ (Figure 3). With the exception of Gd-**2**, these complexes display little variation in $r_{1,on}$. In contrast, $r_{1,off}$ is significantly affected by the linker length. Gd-**4** and Gd-**5** display the lowest value of $r_{1,off}$ (~2.5 mM^{-1} s^{-1}), contributing to their high value of Δr_1. The $r_{1,off}$ values of Gd-**3**, Gd-**6**, and Gd-**7** are notably higher (~3.5–3.8 mM^{-1} s^{-1}), reducing Δr_1 to half that of Gd-**4** and Gd-**5**. $r_{1,off}$ of Gd-**2** is relatively high (~4.5 mM^{-1} s^{-1}) and is not notably increased by the addition of Zn(II) (Δr_1 = 20%). The Δr_1 values resulting from the relatively low values of $r_{1,off}$ suggest that Gd-**4** and Gd-**5** will be the most effective complexes for Zn(II) detection by MRI.

To examine the effect of the field strength on Δr_1 and to determine if the observed changes in r_1 are visible via MRI, T_1-weighted phantom images of Gd-***n*** before and after the addition of Zn(II) were acquired at 7 T (Figure 4). The images and relaxation rates ($R_1 = 1/T_1$) obtained at the higher field strength reflect the trend in Δr_1 observed at 1.4 T. In the absence of Zn(II), images of solutions of Gd-**4** and Gd-**5** are visibly darker compared to the remaining complexes, an observation that can be quantified by the lower R_1 values (Figure 4). The addition of Zn(II) significantly increases image brightness (and R_1 values) for all complexes with the exception of Gd-**2**. Consistent with the $r_{1,on}$ values, the R_1 values and image brightness in the presence of Zn(II) show little variation. However, as with the Δr_1 values, the largest change in image brightness occurs for Gd-**4** and Gd-**5** (Figure 4). This result further confirms that Gd-**4** and Gd-**5** will be the most effective complexes for Zn(II) detection by MRI.

Selectivity and Sensitivity of Gd-*n*. The $r_{1,off}$ values of Gd-***n*** are structurally dependent, while the $r_{1,on}$ values are largely unchanged by linker length variation. This suggests that altering the distance between the Gd(III) chelate and the Zn(II)-binding domain has little effect on either the Zn(II)-binding ability of the complex or the coordination geometry about the Gd(III) center following Zn(II) binding. To explore this hypothesis, the ion selectivity and sensitivity of each Gd-***n*** complex were measured.

The previously reported Zn(II)-activated Gd-***n*** complex (Gd-**3**; Figure 2) was selective for Zn(II) over both Ca(II) and Mg(II). The agent, however, was not selective for Zn(II) over

dx.doi.org/10.1021/ic400681j | *Inorg. Chem.* 2013, 52, 12250–12261

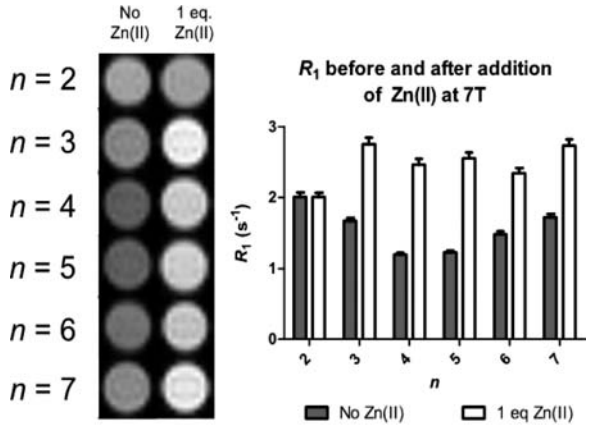

Figure 4. Left: T_1-weighted phantom images of Gd-***n*** before (left) and after (right) the addition of Zn(II). Images were acquired in a HEPES buffer (pH 7.4, 275 μM) at 7 T, 25 °C. In agreement with the r_1 data acquired at 1.4 T, prior to the addition of Zn(II), Gd-**4** and Gd-**5** are darker than the remaining complexes; however, after the addition of Zn(II), there is little variation in brightness between the complexes in which n = 4−7. Right: R_1 values of Gd-***n*** before and after the addition of Zn(II) obtained from T_1-weighted phantom images. The R_1 values from the images acquired at 7 T agree with the relaxivity data obtained at 1.4 T, which indicate that Gd-**4** and Gd-**5** exhibit the largest increase in the relaxation rate upon the addition of Zn(II).

Cu(II) and exhibited a substantial increase in r_1 in the presence of Cu(II). To determine whether the distance between the Zn(II)-binding domain and the Gd(III) chelate affects the selectivity of the agent, the relaxivity of Gd-***n*** was measured in the presence of several concentrations of various metal salts, MCl_2 where M = Zn^{II}, Cu^{II}, Mg^{II}, and Ca^{II} (SI Figure 7).

All Gd-***n*** complexes showed little deviation from the selectivity of Gd-**3**: r_1 increased with increasing concentrations of both Zn(II) and Cu(II) up to 1 equiv. As expected, further addition of M(II) did not affect r_1, suggesting that Gd-***n*** binds one divalent transition metal per complex regardless of the distance between the metal-binding domain and the chelate. The addition of Ca(II) and Mg(II) (up to 3 equiv) had no effect on r_1 for any of the complexes investigated, confirming, as expected, that the selectivity of Gd-***n*** does not depend on the linker length.

The sensitivity of Gd-***n*** is independent of the linker length. The approximate $K_{d,Zn(II)}$ was determined using a competitive binding assay with FluoZin-1, a Zn(II)-activated fluorophore with a known dissociation constant.[22] The $K_{d,Zn(II)}$ of all complexes was within 1 order of magnitude, ranging from ∼10 to 40 μM (SI Figure 5).

In summary, the selectivity and sensitivity experiments indicate that the metal-binding activation event of Gd-***n*** is unaffected by the distance between the Zn(II)-binding domain and the Gd(III) chelate. This is consistent with the observation that $r_{1,on}$ is largely independent of the linker length.

q* Values before and after the Addition of Zn(II).** Although the sensitivity and selectivity of the Gd-n*** complexes are relatively unaffected by the linker length, the Δr_1 values of Gd-***n*** showed a significant structural dependence. Because the Gd-***n*** complexes are designed as q-modulated agents, we expect that the q values of these complexes will reflect the trend in the r_1 values. The q values of each Gd-***n*** complex were measured in both the presence (q_{on}) and absence (q_{off}) of Zn(II), using the lanthanide luminescence lifetimes of the Tb(III) analogues (Tb-**2**−Tb-**7**) in both HEPES buffer (pH 7.4) and deuterated HEPES buffer.

As expected, the relationship between n and the change in the q value in the presence of Zn(II), Δq, mirrors the observed trend in Δr_1, suggesting that variation in Δq is responsible for the structural dependence of Δr_1 (Figure 5). In the absence of Zn(II), the complexes displaying the lowest $r_{1,off}$ (Tb-**4** and Tb-**5**) completely restrict water access to the metal center, displaying a q_{off} of 0.0. The complexes with slightly higher $r_{1,off}$ (Tb-**3**, Tb-**6**, and Tb-**7**) restrict water access less effectively than Tb-**4** and Tb-**5**, as evidenced by their slightly higher q_{off} values (0.2−0.3). Tb-**2** displays the highest q_{off} value, 0.5, consistent with its high $r_{1,off}$. The lack of structural dependence of $r_{1,on}$ is reflected by a similar lack of variation in q_{on}; nearly all complexes have a q_{on} of ∼1.0.

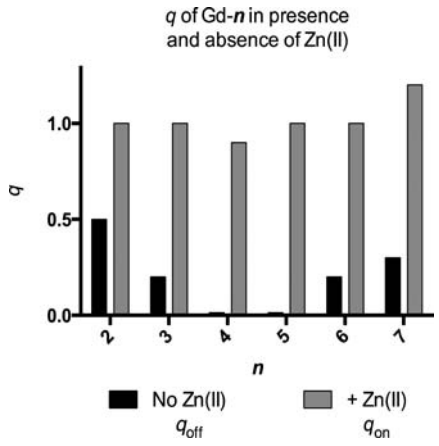

Figure 5. q values of Tb-**2**−Tb-**7** before (q_{off}) and after (q_{on}) the addition of 1 equiv of Zn(II) in HEPES buffer (pH 7.4), 25 °C. The structural dependence of the change in q shows a trend similar to that of Δr_1: Tb-**4** and Tb-**5**, which correspond to the lowest values of $r_{1,off}$, display the lowest values of q_{off}; Tb-**3**, Tb-**6**, and Tb-**7**, which display slightly higher values of $r_{1,off}$, have concomitantly higher values of q_{off}; Tb-**2**, which corresponds to the highest value of $r_{1,off}$, also has the highest q_{off} value. The q_{on} values show little variation, an observation that is reflected by the structural independence of $r_{1,on}$.

The q measurements indicate that the value of n strongly influences the ability of Gd-***n*** to restrict water access to the metal center *prior* to the addition of Zn(II), accounting for the structural dependence of Δr_1. This suggests that, in the absence of Zn(II) (the "off" state), the coordination environment about the metal center depends on the distance between the Zn(II)-binding domain and the Gd(III) chelate. Such a structural dependence is not observed upon bioactivation [Zn(II) addition] of the agent. It is assumed that, in the absence of Zn(II), the acetate groups of the Zn(II)-binding domain coordinate to Gd(III), thereby blocking water access. Consequently, in order to apply information regarding the relationship between Δr_1, q, and n for the Gd-***n*** system to the design and optimization of other classes of bioactivated contrast agents, it is necessary to determine why the linker length alters the ability of the acetate groups of the Zn(II)-binding domain to coordinate Gd(III).

Temperature-Dependent ^{13}C NMR. Eu(III) analogues of Gd(III) contrast agents are commonly employed for structural NMR studies of these complexes.[58−62] The unpaired electrons of Eu(III) broaden and significantly shift the NMR signals of the atoms in close proximity, providing information regarding

which atoms are directly coordinated to the metal center. Moreover, the dynamic behavior of ligand coordination to metals can often be revealed using temperature-dependent NMR. To probe whether the linker length affects coordination of the acetate groups of the Zn(II)-binding domain to the lanthanide center of Gd-***n***, temperature-dependent ^{13}C NMR was performed on Eu(III) analogues of Gd-**2**, Gd-**4**, and Gd-**6**. For each analogue, the β-C atoms of the Zn(II)-binding acetate groups were ^{13}C-labeled (Figure 6).

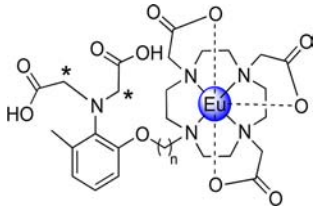

Figure 6. Temperature-dependent NMR was performed on ^{13}C-labeled Eu(III) analogues of Gd-**2**, Gd-**4**, and Gd-**6** to probe how the linker length affects the ability of the acetate groups of the Zn(II)-binding domain to coordinate the lanthanide center. Asterisks indicate ^{13}C-labeled C atoms.

The chemical environment of the two acetate groups is expected to affect the ^{13}C-enriched signals in the ^{13}C NMR spectrum. If neither acetate of the Zn(II)-binding domain is coordinated to the lanthanide, a single ^{13}C-enriched signal with a chemical shift similar to that of the ^{13}C-enriched signal of the free ligand (~65 ppm; SI Figure 9) will be observed. Conversely, if both acetates are coordinated, we would expect to observe a single ^{13}C-enriched peak that is significantly shifted and broadened (compared to the ^{13}C-enriched signal of the free ligand) because of its proximity to the paramagnetic Eu(III) ion. If only one of the acetates is coordinated to the metal center, we would expect to see two different ^{13}C-enriched signals (one of which is sharp and only moderately shifted from the signal of the free ligand and the other both broadened and shifted).

At all temperatures investigated (10, 25, 40, and 60 °C), the ^{13}C NMR spectrum of labeled Eu-**2** shows a single ^{13}C-enriched signal near 60 ppm (Figure 7A), very close to the chemical shift of the ^{13}C-enriched signal of the unmetalated ligand (SI Figure 9). This implies that, in the absence of Zn(II), neither acetate group of the Zn(II)-binding domain coordinates to the metal center (Figure 7A). If the acetate groups are weakly coordinated to the lanthanide ion, the complex cannot effectively restrict water access to the metal center. Thus, this result is consistent with the relatively high q_{off} (0.5) and $r_{1,off}$ (4.8 mM^{-1} s^{-1}) values measured for Gd-**2**.

At low temperatures (10 and 25 °C), the ^{13}C NMR spectrum of labeled Eu-**4** shows two distinct ^{13}C-enriched signals (one sharp signal at 60 ppm and one upshifted, broadened peak near 5 ppm; Figure 7B). As the temperature is increased, the two signals begin to coalesce into a single signal near 30 ppm. Further, this phenomenon is reversible (if the sample is then cooled, the two distinct peaks reappear with the same chemical shifts as before). We hypothesize that at low temperatures one acetate group of the Zn(II)-binding domain is coordinated to the lanthanide center, giving rise to the broadened, down-shifted signal at 5 ppm, while the other acetate remains uncoordinated, accounting for the sharper signal at 60 ppm.

The ^{13}C-enriched peaks of both the unmetalated ligand and Eu-**2** (which displays high values of both q_{off} and $r_{1,off}$, indicating reduced water-restriction capabilities) occur near 60 ppm (Figure 7A and SI Figure 9). This supports the hypothesis that the signal at 60 ppm in the ^{13}C NMR spectrum of labeled Eu-**4** likely arises from an acetate not coordinated to the lanthanide. The significant deviation of the upfield signal from the free ligand acetate correlates to resonance shifting and broadening expected from direct coordination to the lanthanide.

To verify the assignment of the lanthanide-coordinated acetate, an M-**4** analogue was developed in which coordination of the ^{13}C-labeled acetate to the lanthanide could be confirmed. An analogue of Gd-**4**, modified to contain only a single acetate in the Zn(II)-binding domain (**1a**-Gd-**4**), was synthesized and characterized. Similar to Gd-**4** and Gd-**5**, in the absence of Zn(II), the relaxivity of **1a**-Gd-**4** is very low ($r_{1,off}$ = 2.3 mM^{-1} s^{-1}), and the q value of the Tb(III) analogue is 0.0. The effective water-restriction capabilities of **1a**-M-**4** suggest that the single acetate group coordinates directly to the lanthanide.

The ^{13}C-labeled Eu(III) analogue of **1a**-Eu-**4** was synthesized and characterized by temperature-dependent ^{13}C NMR. The ^{13}C NMR spectrum shows a single ^{13}C-enriched signal near 15 ppm that gradually sharpens with increasing temperature (Figure 7C). This supports the hypothesis that the broad upfield signal in the ^{13}C NMR spectrum of Eu-**4** arises from an acetate directly coordinated to the lanthanide. The change in the chemical shift of the upfield signal (5 ppm as opposed to 18 ppm) is likely due to minor differences in the Eu−O bond length because the dipolar contribution to lanthanide-induced changes in the chemical shift shows a strong distance dependence.

It is likely that the two signals in the low-temperature ^{13}C NMR of Eu-**4** arise from acetate groups in two different environments, one coordinated directly to the Eu(III) and the other dissociated from the lanthanide (Figure 7C). We hypothesize that the coalescence of these two signals at higher temperatures results from the increased rate of coordinative exchange of these two acetate groups.

The ^{13}C NMR spectrum of Eu-**6** shares several features with that of Eu-**4** (Figure 7D). At low temperatures (10 °C), two distinct ^{13}C peaks are visible (one broad peak near 5 ppm and one sharp peak near 60 ppm). As with Eu-**4** (Figure 7C), coalescence of these two peaks is observed with increasing temperature. However, this phenomenon occurs at much lower temperatures for Eu-**6**. At 40 °C, the temperature at which relaxivity measurements were made, the two signals have completely coalesced. This suggests that a longer, more flexible linker between the Zn(II)-binding domain and the metal chelate facilitates coordinative exchange of the Zn(II)-binding acetate groups. These data, combined with the reduced water-restriction capability of Gd-**6** (q = 0.2 and r_1 = 3.9), indicate that the acetate exchange process improves water access to the metal, increasing q_{off} and $r_{1,off}$ (Figures 4 and 5).

A total of 1 equiv of Zn(II) was added to each to ^{13}C-labeled analogue of Eu-***n***. In each case, the resulting spectrum contained a single ^{13}C-enriched signal near 60 ppm (SI Figure 8). The chemical shifts of these signals are very similar to those of both the ^{13}C-enriched signal of the unmetalated complexes and the downfield signals in the low-temperature spectra of Eu-**2**, Eu-**4**, and Eu-**6** (Figure 7). This result further supports assignment of the downfield signals in the metalated complexes to acetate groups that are not coordinated to the lanthanide ion. The presence of a single ^{13}C-enriched signal following

dx.doi.org/10.1021/ic400681j | *Inorg. Chem.* 2013, 52, 12250−12261

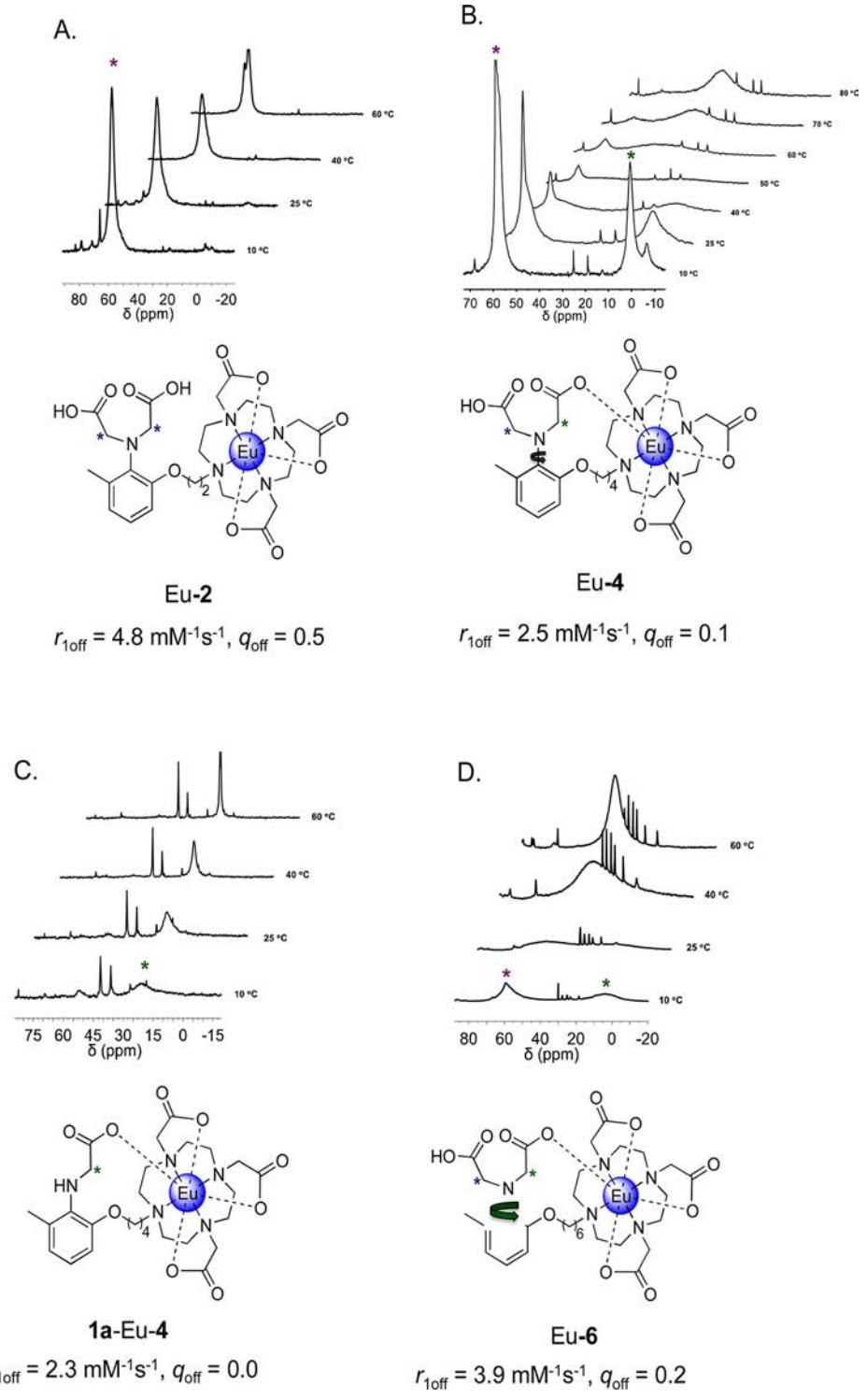

Figure 7. Temperature-dependent ^{13}C NMR spectra of labeled Eu-***n*** complexes. The location of the ^{13}C label is indicated by an asterisk. (A) The spectra of Eu-**2** shows a single ^{13}C-enriched peak, similar in chemical shift to that of the unmetalated ligand. This suggests that neither of the ^{13}C-labeled acetate groups of the Zn(II)-binding domain are coordinated to the lanthanide, leading to high values of q_{off} and $r_{1,off}$. (B) The low-temperature spectra of Eu-**4** show two distinct ^{13}C-enriched peaks, which coalesce into a single peak at higher temperatures. It is thought that the two acetates of the Zn(II)-binding domain are in two different environments. The upfield peak (near 60 ppm and relatively sharp) is thought to arise from a free acetate, while the downfield peak (near 5 ppm and significantly broadened) arises from an acetate that is coordinated to the Eu(III) center. (C) The spectra of **1a**-Eu-**4** show a single ^{13}C-enriched signal near 15 ppm. Because **1a**-Gd-**4** displays excellent water-restriction capabilities, it is thought that the single acetate group of **1a**-Eu-**4** is bound to the Eu(III) center, resulting in a single upfield signal. (D) The spectrum for Eu-**6** is similar to that of Eu-**4**; however, the exchange of the two acetate groups appears to occur at an NMR-observable rate at lower temperatures. Because Gd-**6** shows relatively poor water restriction, it is thought that this increased rate of acetate exchange allows for increased water access to the lanthanide center.

dx.doi.org/10.1021/ic400681j | *Inorg. Chem.* 2013, 52, 12250−12261

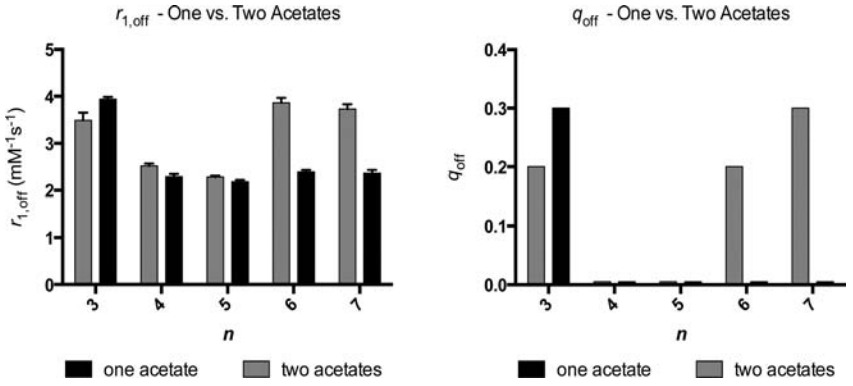

Figure 8. $r_{1,off}$ and q_{off} values of Gd-***n*** complexes containing a Zn(II)-binding domain with only one acetate group (**1a**-Gd-***n***) compared to those of Gd-***n*** (with two acetate groups). In the absence of Zn(II), the relaxivity (left) and q values (right) of **1a**-Gd-***n*** are equal to or lower than those of complexes with Gd-***n***. This confirms that only a single acetate is required to block water access to Gd(III), creating an effective q = 0 state in the absence of the EOI. The significant reduction in $r_{1,off}$ and q_{off} of **1a**-Gd-**6** and **1a**-Gd-7 (in comparison to their two-acetate counterparts) further supports the assertion that exchange of the two acetate groups of the Zn(II)-binding domain reduces the water-restriction capabilities of these complexes.

Zn(II) addition suggests that both acetates bind to the Zn(II) ion, precluding coordination to the lanthanide. Moreover, the sharpness and intensity of the signals suggest that the Zn(II)-binding event significantly increases the distance between the Zn(II)-binding domain and the lanthanide center. In the presence of Zn(II), there is little variation between the ^{13}C-enriched signals of Eu-**2**, Eu-**4**, and Eu-**6**. This is consistent with the observation that $r_{1,on}$ and q_{on} are largely independent of the linker length, as are the sensitivity and selectivity of the complexes.

In summary, the distance between the bioactivated domain [in this case, the Zn(II)-binding domain] and the Gd(III) chelate determines the ability of the acetate groups to coordinate the lanthanide center in the absence of Zn(II). For short linker lengths (n = 2), neither acetate group of the Zn(II)-binding domain is coordinated directly to the metal, facilitating increased water access to the metal center. Complexes with intermediate linker lengths (n = 4) display superior water restriction to Gd(III). For such complexes, only *one acetate* is directly coordinated to the metal at a given time. It is likely that the two acetates undergo coordinative exchange with one another, a process that is accelerated at higher temperatures. Complexes containing long linkers (n = 6) have significantly more coordinative flexibility; consequently, acetate exchange is accelerated at much lower temperatures for such complexes. The $r_{1,off}$ and q_{off} values of M-**6** and M-7 indicate that this accelerated exchange compromises the water-restriction capabilities of these complexes.

Evaluation of 1a-M-*n* Complexes for Elucidation of Design Principles. As previously discussed, the complex with an intermediate linker length (n = 4) and a Zn(II)-binding domain composed of a single acetate group (**1a**-M-**4**) effectively restricts water access to the metal center ($r_{1,off}$ = 2.3 mM^{-1} s^{-1} and q_{off} = 0.0). While such a complex does not bind Zn(II) [and thus cannot be used as a Zn(II)-activated agent in its current form], its behavior provides insight into the structural characteristics required for effective water restriction of q-modulated agents. For example, our laboratory has developed a class of enzyme-activated contrast agents in which a water-blocking moiety is cleaved in the presence of β-glucoronidase.[19] For such agents, any information regarding the factors that influence the efficacy of the water-restricting functional groups (such as how far these groups should be located from the chelate) is valuable, reducing the need for empirical structural optimization of a synthetically challenging system.

^{13}C NMR data suggest that the decrease in water restriction observed for longer linker lengths (n = 6, 7) is the result of facile coordinative exchange of the two acetates of the Zn(II)-binding domain. Thus, it is reasonable to assume that if a single acetate group is sufficient for water restriction, the removal of the second acetate from Gd-**6** and Gd-7 will preclude coordinative exchange, reducing both $r_{1,off}$ and q_{off} and consequently maximizing q-dependent Δr_1. To test this hypothesis, analogues of each complex, modified to contain a single acetate in the Zn(II)-binding domain, were investigated (**1a**-M-***n***, where M = Tb, Gd and n = 3−7) to determine the water-restriction capabilities of the complexes.

The removal of an acetate group from the Zn(II)-binding domain has *no significant effect* on $r_{1,off}$ and q_{off} for complexes with short (**1a**-M-**3**) or intermediate (**1a**-M-**4** and **1a**-M-**5**) linker lengths (Figure 8). Compared to M-**3**, minor increases in both the relaxivity and hydration number (0.5 mM^{-1} s^{-1} and 0.1, respectively) were observed for **1a**-M-**3** in the absence of Zn(II). Relative to the two-acetate analogues, **1a**-M-**4** and **1a**-M-**5** show minor decreases in $r_{1,off}$. Retention of the low values of q and $r_{1,off}$ in single-acetate complexes confirms that only a single acetate is needed for efficient water restriction.

In contrast, removal of an acetate group from complexes with longer linker lengths (**1a**-M-**6** and **1a**-M-7) results in pronounced decreases in both $r_{1,off}$ and q_{off} compared to the M-***n*** counterparts (Figure 8). For both complexes, $r_{1,off}$ decreases from ∼3.9 to ∼2.4 mM^{-1} s^{-1}, while q_{off} decreases to 0.0. This supports the hypothesis that facile coordinative exchange of the Gd-**6** and Gd-7 acetates is responsible for the reduced water-restriction capabilities of these complexes. Moreover, these results elucidate a key principle for the design of bioactivated contrast agents, namely, that the inclusion of a single back-binding acetate increases the window of effective linker lengths for which a sufficiently low relaxivity state can be attained.

■ CONCLUSIONS

The most effective Zn(II)-activated contrast agents (i.e., those displaying the largest value of Δr_1) have a moderate degree of flexibility in the linkage between the Zn(II)-binding domain

dx.doi.org/10.1021/ic400681j | Inorg. Chem. 2013, 52, 12250−12261

and the chelate (where n = 4 or 5; see Figure 4). The Zn(II) sensitivity *and* selectivity of this series of agents is independent of the distance between the chelate and the Zn(II)-binding domain. In contrast, the values of Δq show a strong structural dependence that reflects the trend observed for the Δr_1 values, as would be expected for a q-modulated agent.

Further, the structural dependence of Δr_1 and Δq can be related to the specific coordination geometry about the Gd(III) center that each complex adopts in the *absence* of Zn(II). For complexes displaying the lowest $r_{1,off}$ and q_{off} values (n = 4, 5), only one Zn(II)-binding acetate coordinates to the Gd(III) ion at a given time. The two acetates of the Zn(II)-binding domain undergo coordinative exchange with one another, a process that is accelerated at higher temperatures. Complexes with longer linkers (n = 6, 7) have greater conformational freedom, allowing accelerated coordinative exchange to occur at lower temperatures. The higher q_{off} and $r_{1,off}$ values of these complexes suggest that this accelerated exchange diminishes their water-restriction capabilities.

Removal of one of the Zn(II)-binding acetates has little effect on the $r_{1,off}$ and q_{off} values of Gd-**4** and Gd-**5**. However, for complexes with longer linker lengths (Gd-**6** and Gd-**7**), removal of a single Zn(II)-binding acetate reduces both $r_{1,off}$ and q_{off}. While these complexes do not bind Zn(II) and are thus not applicable as ion-responsive contrast agents, they do provide insight into what structural features are required to effectively restrict water access in the "off" state. The $r_{1,off}$ and q_{off} values of **1a**-Gd-***n*** suggest that (i) only one acetate group is necessary to effectively restrict water access, achieving a sufficiently low relaxivity state in the absence of Zn(II) and (ii) using only a single acetate group to bind back to the Gd(III) center reduces the structural dependence of $r_{1,off}$. Consequently, when designing or improving q-modulated agents that utilize back-binding acetate groups to create a low-relaxivity state prior to the EOI, the use of a single acetate group will increase the number of linker lengths that will result in effective water restriction.

■ ASSOCIATED CONTENT

Ⓢ Supporting Information

Plots used to determine relaxivity values, luminescence lifetime measurements used to determine q values, structure of FluoZin-1, equilibrium used to calculate $K_{d,Zn(II)}$, $K_{d,Zn(II)}$ values, selectivity of Gd-***n*** plots, scheme for the synthesis of Eu-***n****, Eu-***n**** NMR + Zn^{II}, ^{13}C NMR spectra of ^{13}C-labeled ligands **11a**−**11c**, and HPLC retention times and characterization of final complexes. This material is available free of charge via the Internet at http://pubs.acs.org.

■ AUTHOR INFORMATION

Corresponding Author

*E-mail: ratner@northwestern.edu (M.A.R.), tmeade@northwestern.edu (T.J.M.). Phone: 847-491-5652 (M.A.R.), 847-491-2841 (T.J.M.). Fax: 847-491-3832 (T.J.M.).

Notes

The authors declare no competing financial interest.

■ ACKNOWLEDGMENTS

This work was supported by the National Institutes of Health (NIH Grant R01EB005866). Imaging work was performed at the Northwestern University Center for Advanced Molecular Imaging supported by NCI CCSG P30 CA060553 awarded to the Robert H. Lurie Comprehensive Cancer Center. MRI was performed on the 7 T Bruker Pharmascan system purchased with the support of NCRR 1S10RR025624-01. NMR studies were completed at the Northwestern University Integrated Molecular Structure Education and Research Center. A description of the facility and full funding disclosure can be found at http://pyrite.chem.northwestern.edu/analyticalserviceslab/asl.htm. Metal analysis was performed at the Northwestern University Quantitative Bioelemental Imaging Center generously supported by NASA Ames Research Center through Grant NNA04CC36G. M.A.R. thanks the NSF Chemistry Division for support of this work (Grant CHE-1058896). L.M.M. and M.C.H. acknowledge the National Science Foundation Graduate Research Fellowship. J.H.L. acknowledges the Northwestern University Chemistry of Life Processes Lambert Fellowship.

■ REFERENCES

(1) Harney, A. S.; Meade, T. J. *Future Med. Chem.* **2010**, *2*, 503.
(2) Allen, M. J.; Meade, T. J. *Met. Ions Biol. Syst.* **2004**, *42*, 1.
(3) Ostrov, D. A.; Contag, C. H. *Cancer Prev. Res.* **2011**, *4*, 1523.
(4) Matthews, P. M.; Rabiner, I.; Gunn, R. *Curr. Opin. Pharmacol.* **2011**, *11*, 501.
(5) Waldman, A. D.; Jackson, A.; Price, S. J.; Clark, C. A.; Booth, T. C.; Auer, D. P.; Tofts, P. S.; Collins, D. J.; Leach, M. O.; Rees, J. H. *Nat. Rev. Clin. Oncol.* **2009**, *6*, 445.
(6) Rudin, M.; Weissleder, R. *Nat. Rev. Drug Discovery* **2003**, *2*, 123.
(7) Jaffer, F. A.; Weissleder, R. *JAMA, J. Am. Med. Assoc.* **2005**, *293*, 855.
(8) Robles, F. E.; Wilson, C.; Grant, G.; Wax, A. *Nat. Photonics* **2011**, *5*, 744.
(9) Lee, S.; Park, K.; Kim, K.; Choi, K.; Kwon, I. C. *Chem. Commun. (Cambridge, U.K.)* **2008**, 4250.
(10) Bremer, C.; Ntziachristos, V.; Weissleder, R. *Eur. Radiol.* **2003**, *13*, 231.
(11) Hilderbrand, S. A.; Weissleder, R. *Curr. Opin. Chem. Biol.* **2010**, *14*, 71.
(12) Matthews, P. M.; Rabiner, E. A.; Passchier, J.; Gunn, R. N. *Br. J. Clin. Pharmacol.* **2012**, *73*, 175.
(13) Ono, M.; Saji, H. *J. Pharmacol. Sci. (Tokyo, Jpn.)* **2012**, *118*, 338.
(14) Hendricks, J. A.; Keliher, E. J.; Wan, D.; Hilderbrand, S. A.; Weissleder, R.; Mazitschek, R. *Angew. Chem., Int. Ed.* **2012**, *51*, 6813.
(15) Lindner, J. R. *Cardiovasc. Res.* **2009**, *83*, 615.
(16) Ferrara, K. W.; Borden, M. A.; Zhang, H. *Acc. Chem. Res.* **2009**, *42*, 881.
(17) Major, J. L.; Meade, T. J. *Acc. Chem. Res.* **2009**, *42*, 893.
(18) Caravan, P. *Chem. Soc. Rev.* **2006**, *35*, 512.
(19) Duimstra, J. A.; Femia, F. J.; Meade, T. J. *J. Am. Chem. Soc.* **2005**, *127*, 12847.
(20) Li, W.-h.; Fraser, S. E.; Meade, T. J. *J. Am. Chem. Soc.* **1999**, *121*, 1413.
(21) Louie, A. Y.; Huber, M. M.; Ahrens, E. T.; Rothbacher, U.; Moats, R.; Jacobs, R. E.; Fraser, S. E.; Meade, T. J. *Nat. Biotechnol.* **2000**, *18*, 321.
(22) Major, J. L.; Parigi, G.; Luchinat, C.; Meade, T. J. *Proc. Natl. Acad. Sci. U.S.A.* **2007**, *104*, 13881.
(23) Caravan, P. *Chem. Soc. Rev.* **2006**, *35*, 512.
(24) Moats, R. A.; Fraser, S. E.; Meade, T. J. *Angew. Chem., Int. Ed. Engl.* **1997**, *36*, 726.
(25) Alauddin, M. M.; Louie, A. Y.; Shahinian, A.; Meade, T. J.; Conti, P. S. *Nucl. Med. Biol.* **2003**, *30*, 261.
(26) Urbanczyk-Pearson, L. M.; Femia, F. J.; Smith, J.; Parigi, G.; Duimstra, J. A.; Eckermann, A. L.; Luchinat, C.; Meade, T. J. *Inorg. Chem. (Washington, D.C.)* **2008**, *47*, 56.
(27) Yoo, B.; Pagel, M. D. *J. Am. Chem. Soc.* **2006**, *128*, 14032.
(28) Yoo, B.; Raam, M. S.; Rosenblum, R. M.; Pagel, M. D. *Contrast Media Mol. Imaging* **2007**, *2*, 189.

(29) Li, Y.; Sheth, V. R.; Liu, G.; Pagel, M. D. *Contrast Media Mol. Imaging* **2010**.
(30) Major, J. L.; Boiteau, R. M.; Meade, T. J. *Inorg. Chem.* **2008**, *47*, 10788.
(31) Que, E. L.; Chang, C. J. *J. Am. Chem. Soc.* **2006**, *128*, 15942.
(32) Li, W.-h.; Parigi, G.; Fragai, M.; Luchinat, C.; Meade, T. J. *Inorg. Chem.* **2002**, *41*, 4018.
(33) Que, E. L.; Gianolio, E.; Baker, S. L.; Aime, S.; Chang, C. J. *Dalton Trans.* **2010**, *39*, 469.
(34) Esqueda, A. C.; Lopez, J. A.; Andreu-de-Riquer, G.; Alvarado-Monzon, J. C.; Ratnakar, J.; Lubag, A. J. M.; Sherry, A. D.; De Leon-Rodriguez, L. M. *J. Am. Chem. Soc.* **2009**, *131*, 11387.
(35) Lubag, A. J. M.; De Leon-Rodriguez, L. M.; Burgess, S. C.; Sherry, A. D. *Proc. Natl. Acad. Sci. U.S.A.* **2011**, *108*, 18400.
(36) Lowe, M. P.; Parker, D.; Reany, O.; Aime, S.; Botta, M.; Castellano, G.; Gianolio, E.; Pagliarin, R. *J. Am. Chem. Soc.* **2001**, *123*, 7601.
(37) Aime, S.; Barge, A.; Botta, M.; Howard, J. A. K.; Kataky, R.; Lowe, M. P.; Moloney, J. M.; Parker, D.; de Sousa, A. S. *Chem. Commun. (Cambridge, U.K.)* **1999**, 1047.
(38) Hall, J.; Haener, R.; Aime, S.; Botta, M.; Faulkner, S.; Parker, D.; de Sousa, A. S. *New J. Chem.* **1998**, *22*, 627.
(39) Wu, Y.; Soesbe, T. C.; Kiefer, G. E.; Zhao, P.; Sherry, A. D. *J. Am. Chem. Soc.* **2010**, *132*, 14002.
(40) Liu, G.; Li, Y.; Sheth, V. R.; Pagel, M. D. *Mol. Imaging* **2012**, *11*, 47.
(41) Tweedle, M. F. *Invest. Radiol.* **1992**, *27*, 2.
(42) Urbanczyk-Pearson, L. M.; Femia, F. J.; Smith, J.; Parigi, G.; Duimstra, J. A.; Eckermann, A. L.; Luchinat, C.; Meade, T. J. *Inorg. Chem.* **2008**, *47*, 56.
(43) Urbanczyk-Pearson, L. M.; Meade, T. J. *Nat. Protoc.* **2008**, *3*, 341.
(44) Kim, B.-J.; Kim, Y.-H.; Kim, S.; Kim, J.-W.; Koh, J.-Y.; Oh, S.-H.; Lee, M.-K.; Kim, K.-W.; Lee, M.-S. *Diabetes* **2000**, *49*, 367.
(45) Barnham, K. J.; Bush, A. I. *Curr. Opin. Chem. Biol.* **2008**, *12*, 222.
(46) Viles, J. H. *Coord. Chem. Rev.* **2012**, *256*, 2271.
(47) Sensi, S. L.; Paoletti, P.; Bush, A. I.; Sekler, I. *Nat. Rev. Neurosci.* **2009**, *10*, 780.
(48) Takeda, A.; Hirate, M.; Tamano, H.; Oku, N. *Epilepsy Res.* **2003**, *54*, 123.
(49) Bhatt, A.; Farooq Muhammad, U.; Enduri, S.; Pillainayagam, C.; Naravetla, B.; Razak, A.; Safdar, A.; Hussain, S.; Kassab, M.; Majid, A. *Stroke Res. Treat.* **2011**, *2010*, 245715.
(50) Koh, J.-Y.; Suh, S. W.; Gwag, B. J.; He, Y. Y.; Hsu, C. Y.; Choi, D. W. *Science (Washington, D.C.)* **1996**, *272*, 1013.
(51) Lee, J. M.; Zipfel, G. J.; Park, K. H.; He, Y. Y.; Hsu, C. Y.; Choi, D. W. *Neuroscience (Oxford, U.K.)* **2002**, *115*, 871.
(52) Ghosh, S. K.; Kim, P.; Zhang, X.-a.; Yun, S.-H.; Moore, A.; Lippard, S. J.; Medarova, Z. *Cancer Res.* **2010**, *70*, 6119.
(53) Franklin, R. B.; Feng, P.; Milon, B.; Desouki, M. M.; Singh, K. K.; Kajdacsy-Balla, A.; Bagasra, O.; Costello, L. C. *Mol. Cancer* **2005**, *4*, 32.
(54) Mastarone, D. J.; Harrison, V. S. R.; Eckermann, A. L.; Parigi, G.; Luchinat, C.; Meade, T. J. *J. Am. Chem. Soc.* **2011**, *133*, 5329.
(55) Strauch, R. C.; Mastarone, D. J.; Sukerkar, P. A.; Song, Y.; Ipsaro, J. J.; Meade, T. J. *J. Am. Chem. Soc.* **2011**, *133*, 16346.
(56) Quici, S.; Cavazzini, M.; Marzanni, G.; Accorsi, G.; Armaroli, N.; Ventura, B.; Barigelletti, F. *Inorg. Chem.* **2005**, *44*, 529.
(57) Gee, K. R.; Zhou, Z. L.; Ton-That, D.; Sensi, S. L.; Weiss, J. H. *Cell Calcium* **2002**, *31*, 245.
(58) Miller, K. J.; Saherwala, A. A.; Webber, B. C.; Wu, Y.; Sherry, A. D.; Woods, M. *Inorg. Chem.* **2010**, *49*, 8662.
(59) Carney, C. E.; Tran, A. D.; Wang, J.; Schabel, M. C.; Sherry, A. D.; Woods, M. *Chem.—Eur. J.* **2011**, *17*, 10372.
(60) Mani, T.; Tircso, G.; Zhao, P.; Sherry, A. D.; Woods, M. *Inorg. Chem.* **2009**, *48*, 10338.
(61) Woods, M.; Kovacs, Z.; Kiraly, R.; Bruecher, E.; Zhang, S.; Sherry, A. D. *Inorg. Chem.* **2004**, *43*, 2845.
(62) Woods, M.; Kovacs, Z.; Zhang, S.; Sherry, A. D. *Angew. Chem., Int. Ed.* **2003**, *42*, 5889.